Acta Materialia 179 (2019) 414–423

Contents lists available at ScienceDirect

Acta Materialia

journal homepage: www.elsevier.com/locate/actamat

Full length article

In-situ quantitative TEM investigation on the dynamic evolution of individual twin boundary in magnesium under cyclic loading

Bo-Yu Liu [a], K. Eswar Prasad [a, b, **], Nan Yang [a], Fei Liu [a], Zhi-Wei Shan [a, *]

[a] Center for Advancing Materials Performance from the Nanoscale (CAMP-Nano) & Hysitron Applied Research Center in China (HARCC), State Key Laboratory for Mechanical Behavior of Materials, Xi'an Jiaotong University, Xi'an, 710049, People's Republic of China

[b] Discipline of Metallurgy Engineering and Materials Science, Indian Institute of Technology Indore, Simrol, Indore, 453552, India

A R T I C L E   I N F O

Article history:
Received 18 November 2018
Received in revised form
19 August 2019
Accepted 23 August 2019
Available online 28 August 2019

Keywords:
Twinning and detwinning
Twin boundary migration
Tension-compression asymmetry
Magnesium
In-situ TEM

A B S T R A C T

Quantification of dynamics of individual twin boundary (TB) migration such as the velocities and corresponding stresses, is of critical importance for understanding the deformation behavior of magnesium alloys. By conducting *in-situ* cyclic loading experiments on submicron magnesium pillars inside transmission electron microscope (TEM), the dynamics of individual TB migration and the associated twinning-detwinning phenomena are systematically investigated. It is found that the TB can migrate forward and backward under each cyclic loading paths, corresponding to the twinning-detwinning cycles. The TB morphology changes constantly during its migration. Surprisingly, the stress required for TB migration is found to be higher in compression than in tension, and the TB migration velocity in compression is slower than in tension. Such asymmetry is proposed to be associated with different defect environment on either side of TB and the TB structure per se. The considerable amount of energy absorbed during the TB migration is believed to account for at least part of the good damping properties of Mg. Our results are also expected to benefit the modeling of deformation twinning behavior in Mg and other HCP metals.

1. Introduction

In metals with hexagonal close packed (HCP) crystal structure, deformation twinning (DT), besides dislocation slip, is an important deformation mode that accommodates plastic deformation [1–3]. In magnesium (Mg), a typical lightweight HCP metal with promising applications in aerospace and automotive industries, the most commonly observed DT mode is $\{10\bar{1}2\}$ extension twinning [4]. The DT leads to creation of interfaces, called as twin boundaries (TBs), between the parent matrix and twinned regions with a definite crystallographic relation. The $\{10\bar{1}2\}$ twins in Mg can grow or shrink through the migration of TBs accommodating significant amount of plastic strain by twinning shear [2] or unit cell reconstruction [5,6]. Besides generating plastic strain, the migrating TBs also influences the work hardening behavior by interacting with lattice dislocations, other twin lamellae, grain boundaries, and second phase particles [7–16]. In addition, the forward and backward migration of TBs also referred to as twinning and detwinning, respectively, under cyclic loading are expected to be beneficial for increasing the damping capacity of Mg alloys [17,18].

Since TB migration has a considerable influence on the plastic deformation of Mg alloys, there is a pressing need for quantitative description of dynamics of TB migration, such as the TB migration velocities (V_{TB}) and corresponding stresses, for improved understanding of deformation behavior of Mg alloys and develop robust plasticity models that can accurately capture the physics of deformation. However, to authors' knowledge, limited number of studies have been performed in quantifying TB migration in Mg due to the challenges associated with TB tracking and the determination of stress needed for TB migration. In bulk scale samples, profuse twins will be generated under mechanical loading and the twins can interact with each other, which makes the tracking of individual TBs and stress analysis very difficult [19–21]. Efforts have been made to study the DT behavior in real time inside transmission electron microscope (TEM), but stresses associated with TB

* Corresponding author.
** Corresponding author. Center for Advancing Materials Performance from the Nanoscale (CAMP-Nano) & Hysitron Applied Research Center in China (HARCC), State Key Laboratory for Mechanical Behavior of Materials, Xi'an Jiaotong University, Xi'an, 710049, People's Republic of China.
E-mail addresses: eswar@iiti.ac.in (K.E. Prasad), zwshan@xjtu.edu.cn (Z.-W. Shan).

https://doi.org/10.1016/j.actamat.2019.08.043
1359-6454/

migration were not quantified [22,23]. Recently, an *in-situ* tensile test on polycrystalline Mg inside a scanning electron microscope (SEM) has been performed to study the individual TB migration, which reported a V_{TB} of ~35 nm/s under an external applied stress of about 35 MPa [24]. But such measured stress reflects the collective mechanical response of several grains. Therefore, precise determination of stress applied on a certain TB is difficult in such polycrystalline sample. The *in-situ* TEM pillar compression tests on Mg single crystals with specially designed orientation allow the activation of a single twin variant, which enable the real time observation of individual TB migration and measure corresponding stresses [5,25,26]. However, such monotonic compression tests do not allow to investigate the backward migration of TBs. In the current study, we have systematically investigated the migration of an individual $\{10\bar{1}2\}$ TB in Mg pillars by performing *in-situ* TEM cyclic loading experiments. The crystal orientations on either side of the TB are chosen in such a way that the TB migration is the predominant deformation mechanism under both tension and compression.

2. Experimental methods

2.1. Sample fabrication

The material used in the present study was made from 99.99% pure Mg single crystal disks (12 mm in diameter and 1 mm in thickness) obtained from GermanTech Co. Ltd. The disk was cut into thin rectangular specimens using electrical discharge machining so as to avoid the machining induced damage. The specimens were further reduced to a thickness of about 100 μm by gentle polishing on high grit emery paper. One end of this rectangular specimen was electrochemically polished to thickness of 5–10 μm. Submicron size pillars with dog-bone shape were then fabricated using focused ion beam (FIB) machining following the procedure adopted by Liu et al. [5]. Extreme care was exercised to mitigate the damage due to Gallium ions.

Since the objectives of the current study are to systematically investigate the role of TB migration on the deformation under cyclic loading conditions as well as to characterize the TB velocity, the specimens were designed in such a way that the gauge section of the specimen contains a single TB. There are two ways in which the TB can be introduced in the gauge section of the specimen: In the first method, the submicron specimen can be loaded beyond the yield limit to generate large number of twins (and hence TBs) [27], but the twins introduced by this method are very random thus defying the objective of this study. While in the second method, submicron specimens can be fabricated around a pre-existing twin that has already been introduced during the metallographic polishing stage (Note that due to low critical resolved shear stress (CRSS), $\{10\bar{1}2\}$ twins are always present in the as-polished samples [24]). The latter method is advantageous as it facilitates the observation of a single TB although it requires extensive and careful survey of the entire specimen to locate the TB. Nevertheless, TB can be identified using ion-induced secondary electron imaging mode as it provides marked contrast between parent and twin lattices due to the difference in crystal orientations [28].

Fig. 1a shows the contrast between two grains separated by a twin boundary. Specimens are fabricated from the region indicated in dotted line using FIB machining in such a way that the boundary is in the gauge section. The TEM image of the dog-bone shaped specimen and selected area electron diffraction patterns (SADPs) acquired from the upper and lower grains are shown in Fig. 1b. The zone axis (ZA) for the two grains are $\sim\langle\bar{1}2\bar{1}\bar{3}\rangle$ and $\sim\langle 2\bar{1}\bar{1}0\rangle$, respectively. The prismatic $\{1\bar{1}00\}$ plane of the upper grain is approximately parallel to the basal $\{0002\}$ plane of the lower grain. This specific orientation relationship can be regarded as $\{10\bar{1}2\}$ twin orientation. Therefore, the boundary separating the two regions should be a $\{10\bar{1}2\}$ TB. The crystallographic orientations of the twin and matrix are represented by the HCP unit cells in Fig. 1a.

2.2. In-situ mechanical testing

The sample is then taken to TEM for mechanical testing and a schematic illustrating the loading configuration is shown in Fig. 2. The *in-situ* mechanical testing is performed using a Hysitron PicoIndenter (PI95) inside a TEM (JEOL 2100F, 200 keV). One end of the specimen is held by a diamond tensile grip or a diamond flat punch in tension or compression test, respectively. All the experiments are conducted under displacement control which yields a strain rate of ~10^{-3}/s for the given specimen dimensions. However, due to thermal drift of loading device, the actual displacement rate (measured from the *in-situ* videos) applied on samples slightly deviates from the set value (as given in Table A1) leading to slight variation in strain rate. This effect will be considered when

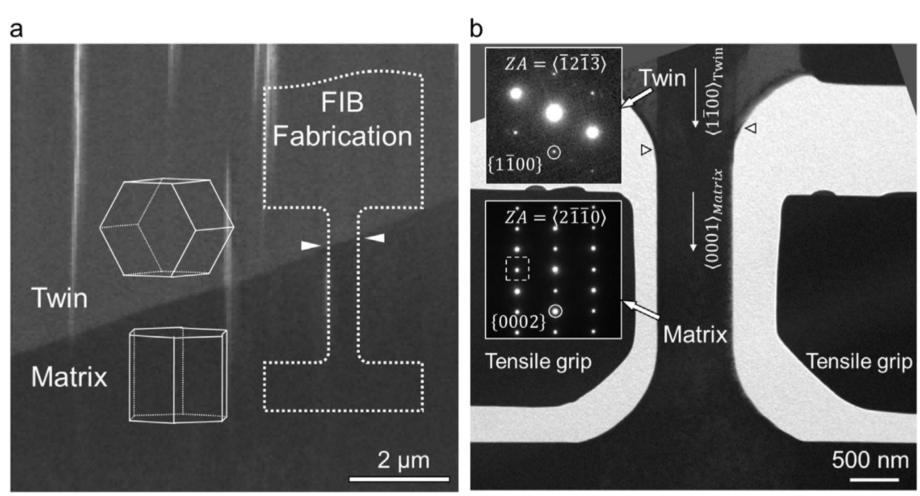

Fig. 1. (a) Microstructure obtained using ion-induced secondary electron imaging clearly illustrating the contrast between the twin and matrix separated by a TB. The inset HCP frames describe the crystal orientations of matrix and twin. The dog-bone shape pillar (highlighted by the dashed frame) with the TB lying in the gauge section is fabricated by FIB. (b) TEM bright field image showing an as fabricated sample along with the SADPs acquired for the twin and matrix regions. The position of TB is marked by a pair of arrow heads.

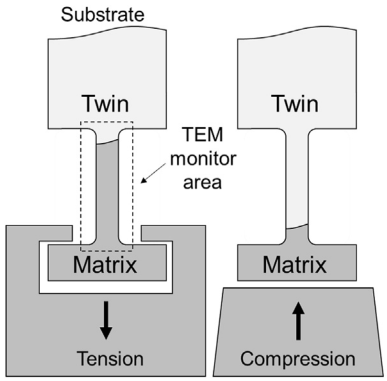

Fig. 2. Schematics illustrating the tension and compression loading setups.

discussing the V_{TB} in section 4.4.

Supplementary video related to this article can be found at https://doi.org/10.1016/j.actamat.2019.08.043

The imaging condition during the deformation is key in clearly demarcating the twin and matrix. Dark field imaging condition is used throughout the in-situ mechanical testing, which illuminates the matrix region (bright in contrast) while makes the twin region appears as dark thereby highlighting the boundary between them as shown in Fig. 3. A **g** vector $\{0\bar{1}10\}_{Matrix}$ is chosen to perform the dark field imaging, because this diffracted spot appears only in the SADP of matrix but not in twin, as marked by the dashed block in Fig. 1b.

During the tensile loading, the tensile grip moves downward i.e., along the $\langle 0001\rangle_{Matrix}$, exerting a net tensile force on the TB which causes it to move downward. While during the compression loading, the diamond punch travels in the upward direction along $\langle\bar{1}100\rangle_{Twin}$, resulting a net compressive force on the TB and causing it to move upward. We refer the TB movement under tension (twin growth) and compression (twin shrink) as twinning and detwinning, respectively. The TB migration in the gauge portion is continuously monitored by a Gatan 833 camera at a frame rate of 10 frames per second. The load is applied till the TB moves from one end of the gauge length to the other end. Since the contrast of TB is fuzzy near the end of the gauge part, it is difficult to precisely decide when the loading should be terminated. Therefore, the initial and final positions of the TB are different in each cycle. In addition, the TEM observation is confined to sample gauge length, while the contact between loading device and specimen is not monitored. Therefore, the position of the loading device at the start of each cycle cannot be exactly the same, and the redundant displacement of the indenter before it actually starts applying load would be different in each cycle. These effects resulted in different strain values during each cycle although the programmed displacement is the same.

Four sets of experiments were performed to obtain repeatable and reproducible results. In order to study if the loading sequence would affect the V_{TB}, we used two types loading sequences: For one type, the cyclic loading started with tension first followed by the compression and so on (i.e. tension, compression, tension …); while for the other type, the cyclic loading started with compression first followed by tension and so on (i.e. compression, tension, compression …), as shown in Table A1. In all the experiments, the cyclic loading test was terminated when TB was not clearly visible. This could be due to the poor diffraction contrast arising because of the out of plane deformation of the specimen. The yield stress and V_{TB} data for these loading cycles were not considered for subsequent analyses.

3. Results

3.1. Reversible TB migration under cyclic loading

Irrespective of the loading sequence, reversible migration of TB is observed during cycling loading. Fig. 3 indicates the start and finish positions of a TB on a sample subjected to cyclic loading in the sequence of 1-Tension, 2-Compression, 3-Tension, 4-Compression and 5-Tension (Sample #1). For the given loading conditions, Schmid analysis suggests that, $\{10\bar{1}2\}$ twinning is favorable in the matrix region under tension, while under compression it is favorable in the twin region. It is observed that the plastic deformation occurs by the migration of existing TB rather than nucleation of new twins. This could be due to the low TB migration stress as compared to high twin nucleation stress. The tensile loading caused downward migration of TB resulting in the growth of twin region at the expense of matrix region. The region through which the TB had migrated underwent a change in crystallographic orientation of about 90° with respect to the initial orientation. Therefore, in this reoriented lattice, the load reversal (i.e. compression) will promote detwinning thereby causing the TB to migrate upward. During the reverse TB migration, the matrix region grew at the expense of twin region. The alternating tension-compression loading cycles caused forward and reverse TB migration (also known as twinning and detwinning) due to the continuous exchange of twin/matrix regions.

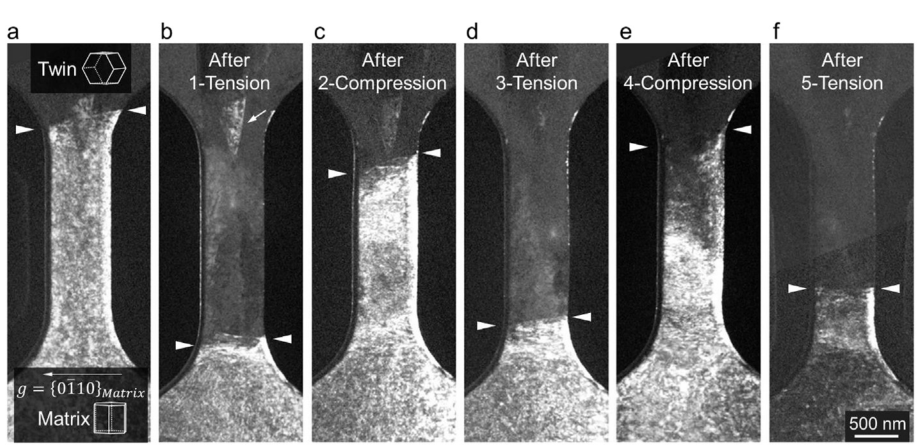

Fig. 3. TEM dark field images showing the position of TB in the (a) undeformed sample and (b–f) at the end of each loading cycle. The TB is marked by a pair of white arrow heads at both the edges to guide the eye. The ZA for twin and matrix are $\sim\langle\bar{1}2\bar{1}\bar{3}\rangle$ and $\sim\langle 2\bar{1}\bar{1}0\rangle$, respectively. The g vector is $\{0\bar{1}10\}_{Matrix}$, as marked by the dashed block in the SADP in Fig. 1b.

3.2. The mechanical response

The engineering stress, σ *vs.* engineering strain, ε curves shown in Fig. 4 are characterized by initial elastic region, where the σ linearly varies with ε, followed by a plateau region. This plateau region is typically associated with TB migration. The yield strength for each of the loading cases was identified as the value at which stress unambiguously deviates from linearity in the σ *vs.* ε curve. We found that 0.5% proof stress gave a reasonable estimate of this as shown in Fig. 4 and listed in Table 1. Recent studies showed that the formation of new twins usually accompanied by strain bursts and stress drops [5,29]. Such strain burst and stress drops were not noticed in the σ *vs.* ε curves shown in Fig. 4, indicating that no new twins have nucleated either during tension or compression, which is also supported by the *in-situ* video. Note that in the 4-Compression, the σ *vs.* ε curve shows an abrupt increase in σ with ε after the plateau region. A careful examination of the *in-situ* video revealed that during this loading, the TB moved out of the gauge section and reached the grip section of the sample. After that, the plasticity could only be accommodated by non-basal dislocation slips that required high CRSS, thereby resulting in an abrupt increase in $d\sigma/d\varepsilon$. Few other interesting observations could be noted from the *in-situ* video and the corresponding σ *vs.* ε curves: (i) At the end of each loading, there is a slight recovery of the TB which could be due to adhesive forces between the pillar surface and loading device, or the relaxation of back stress (may be imposed by the dislocations) ahead of the TB; (ii) TB starts to move, albeit small, well before the yield stress suggesting that the local stresses near the TB may be higher than the macroscopic stress; (iii) Sometimes TB migration was characterized by jerky motion.

3.3. The morphology of migrating TB

Snapshots captured from *in-situ* video show typical morphologies of the migrating TB during each loading test (Fig. 5). At this juncture it is important to assess the geometry of the TB: In a square pillar with the geometry and crystallographic orientation described in Fig. 1 (front surface and back surface are perpendicular to $\langle\bar{1}2\bar{1}\bar{3}\rangle_{Twin}$ and $\langle 2\bar{1}\bar{1}0\rangle_{Matrix}$, the pillar axial direction and loading direction are parallel to $\langle\bar{1}100\rangle_{Twin}$ and $\langle 0001\rangle_{Matrix}$), the configuration of a planar $\{10\bar{1}2\}$ coherent TB (CTB) is shown in the supplementary Fig. A1. For a planar CTB, the intersection between TB and front and back surfaces should be two parallel straight lines. When viewed along the zone axis of $\langle\bar{1}2\bar{1}\bar{3}\rangle_{Twin}$ and $\langle 2\bar{1}\bar{1}0\rangle_{Matrix}$ (as in Figs. 1, 3 and 5), the angle between such intersection lines and horizontal line should be ~26.5°. In Figs. 3 and 5, the dark/bright boundary should be the "*Upper intersection*" line because above this line there should be no matrix volume. Therefore, if the TB is a planar CTB, the bright/dark boundary should be a straight line with 26.5° inclined from the horizontal line. However, the boundary is not straight but corrugated, and the shape of this boundary changes continuously during its migration. It can be argued from the above discussion as well from Fig. 5 that the TB is not planar but rugged in nature, indicating that the TB observed here is not a perfect $\{10\bar{1}2\}$ CTB. Such non-planar TB morphology is frequently observed in Mg [5,6,30,31], which could be attributed to the presence of profuse prismatic-basal (PB), basal-prismatic (BP), and prismatic-prismatic interfaces on the $\{10\bar{1}2\}$ TB.

Another interesting observation from *in-situ* video is the continuous change of TB morphology during its forward and backward migration, which seems like flow of water through a hollow tube. It also appears as some parts of the TB moves faster than the others. The observed TB morphology evolution may be influenced by local stress field, which needs further investigation. This nature of TB motion may have a marked influence on the way in which the TBs interact with different defects: It may allow migrating TBs to easily surmount the short-range obstacles (e.g. point defects and scattered dislocations) while encountering difficulty in overcoming the long-range obstacles (e.g. planar defects such as GB and TBs, volume defects such as precipitates, and forest of dislocations). Liu et al. [16] found that TB can easily pass through particle-shape or rod-shape precipitates, while a dense distribution

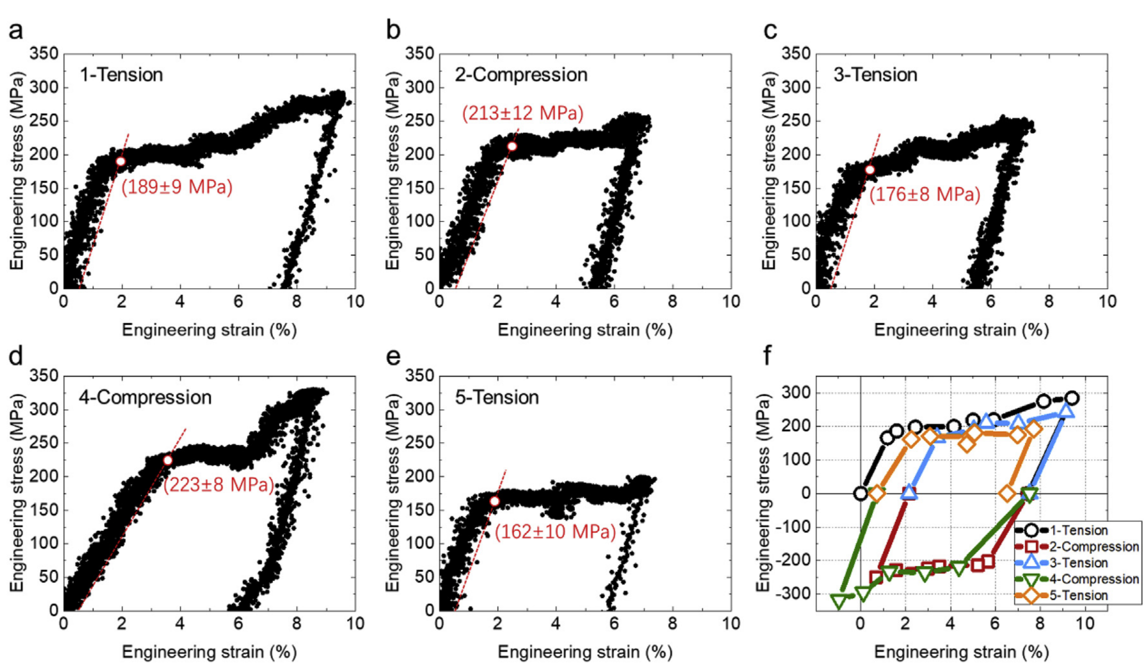

Fig. 4. Engineering stress *vs.* strain curves of five consecutive loadings of Sample #1. (a) 1-Tension; (b) 2-Compression; (c) 3-Tension; (d) 4-Compression; (e) 5-Tension. The yield stress is defined as the stress at 0.5% offset strain values, as indicated by the red line. A summary of all curves is plotted in (f) in the same axis for comparison. (For interpretation of the references to colour in this figure legend, the reader is referred to the Web version of this article.)

Table 1
Mechanical data for each loading cycle of Sample #1.

Loading	Yield stress (MPa)	Strain hardening exponent, n (in the plateau region)	Work hardening rate (in the plateau region), $d\sigma/d\varepsilon$ (MPa)	Energy dissipation ($\times 10^6$ J/m^3)
1-Tension	189 ± 09	0.12	834 ± 235	16.78
2-Compression	213 ± 12	0.07	442 ± 168	11.06
3-Tension	176 ± 08	0.11	823 ± 246	10.92
4-Compression	223 ± 08	0.09	420 ± 103	14.32
5-Tension	162 ± 10	0.08	391 ± 174	9.62

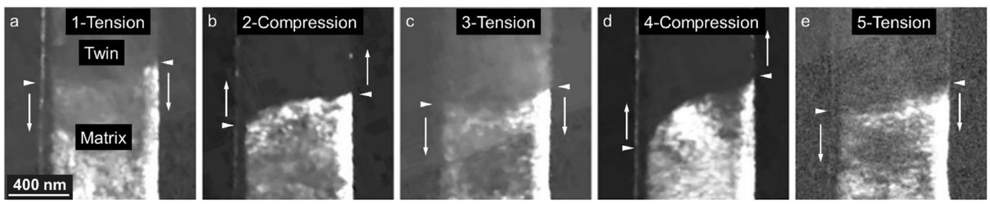

Fig. 5. Snapshots captured from the *in-situ* video at different time intervals clearly showing the non-planar morphology of the migrating TB in (a) 1-Tension, (b) 2-Compression, (c) 3-Tension, (d) 4-Compression and (e) 5-Tension, respectively. TB migration directions are indicated by white arrows. The zone axis and dark field imaging condition are same to those used in Fig. 3.

of plate like precipitates offers more resistance for TBs, analogous to regulation of water flow through a dam, resulting in an increase in strength.

3.4. Determination of TB migration velocity V_{TB}

The average V_{TB} is obtained from the linear slope of TB displacement *vs*. time plot following the procedure described in Ref. [24]. Due to the non-planarity of the TB (as shown in Fig. 5), TB displacement is measured at the left end, center point and right end of the TB, and the average value is taken to calculate the V_{TB}. The V_{TB} at each test are listed in Table A1. Note that the V_{TB} in tensile loading (twinning) is higher than that in compressive loading (detwinning). Such tension-compression asymmetry is discussed in detail in later sections.

4. Discussion

The current experimental results provide important insights into the role of TB migration on the deformation behavior of Mg as the majority of the plastic flow occurs due to the migration of an individual TB. This allows in better understanding of DT mediated plasticity, kinetics of TB migration, tension-compression asymmetry, and energy absorption characteristics associated with TB migration.

4.1. Strain component analyses

In order to determine whether the plastic deformation of the tested samples is mainly mediated by DT, we carried out the *strain component analysis* [16] to evaluate the contribution of TB migration mediated strain to the total plastic strain. The total plastic strain, ε_p is the sum of plastic strain due to TB migration, ε_{tw} and dislocation slip, ε_{sl}, i.e. $\varepsilon_p = \varepsilon_{tw} + \varepsilon_{sl}$. The $\{10\bar{1}2\}$ DT results in a lattice reorientation, generating ~6.4% strain along the *c*-axis (the axial direction of the dog-bone specimen). Therefore, the nominal plastic strain due to DT can be estimated by multiplying 6.4% strain with the volume through which the TB has migrated (f_{tw}), $\varepsilon_{tw} = f_{tw} \times 6.4\%$. Since the TEM image only provides 2D projection, the volume fraction can be estimated by area fraction multiplied by sample thickness. The dislocation slip mediated plasticity, ε_{sl} can then be obtained by subtracting ε_{tw} from ε_p. The total plastic strain, ε_p, can be obtained from the stress *vs*. strain curves (can also be measured from the TEM images of the initial and deformed pillar). The strain partitioning is plotted in Fig. 6 clearly indicates that the majority of the contribution to ε_p comes from ε_{tw}.

Although TB migration is the primary deformation mode, the contribution from dislocation slip cannot be eliminated. The contribution to ε_{sl} can come from interaction of pre-existing mobile dislocations or activation of new dislocation slip systems. Possible active dislocation slip systems can be estimated by performing Schmid factor analysis, as described in detail in section 4.4.2. After the entire gauge length is consumed by the twin, further plastic strain is primarily accommodated by ε_{sl}. In addition to the direct contribution to plastic straining, dislocations can also influence the plastic deformation by impeding the migrating TB. This may partly account for the observed slight strain hardening in the plateau region on stress *vs*. strain curves (Fig. 4).

4.2. Work hardening during TB migration

It is also important to examine the work hardening behavior in the plateau region. The work hardening rate, $d\sigma/d\varepsilon$, and strain hardening exponent, n, in the plateau regime are quantified using

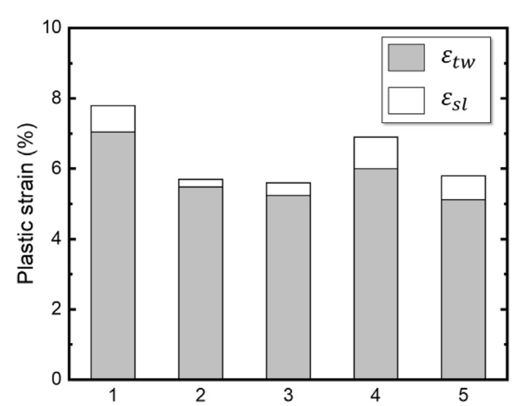

Fig. 6. Variation of plastic strain along with the contributions of plastic strain due to twinning, ε_{tw} and dislocation slip, ε_{sl} plotted against each loading cycle of Sample #1. The figure confirms that the majority of the contribution to plastic flow is due to TB migration.

power law and presented in Table 1. A slightly higher $d\sigma/d\varepsilon$ is observed in tension (at least for the first two cycles) compared to the compression, suggesting an increased resistance to the TB migration, or more dislocation multiplication and interaction. The $d\sigma/d\varepsilon$ is found to decrease with increasing number of cycles. This can probably be attributed to the mechanical annealing observed due to cyclic deformation according to which the dislocations near the surface tend to move out of the pillar due to high image forces [32]. The hardening rate during compression is a small value to start with. Therefore the mechanical annealing will not have much effect on the decrease in hardening rate. In general, the observed strain hardening, albeit small, is presumably related to the interaction between TB and dislocations [33–37], and to the behaviors of dislocations per se (e.g. dislocation nucleation from pillar surface [29] or escape to pillar surface [32], and dislocations generated from TB [38,39]). However, in the current stage, it is difficult to simultaneously capture the dislocation activity and TB migration in *in-situ* TEM mechanical testing. The real time TB-dislocation interaction is definitely worth for further study.

4.3. TB migration rates

In our experiments, the samples are deformed under strain rate of ~10^{-3}/s and the measured V_{TB} is in the range of 42–86 nm/s (Table A1). This is higher than the V_{TB} (~35 nm/s) reported in a previous study conducted at a lower strain rate of ~10^{-4}/s [24]. A much higher V_{TB}, about 12–30 m/s (nine orders of magnitude higher than the current experiments), is observed under high strain rate (~10^3/s) deformation experiments [21]. This indicates the fact that V_{TB} increases with increasing strain rate. Such strain rate dependence can be attributed to the following: The contribution of DT to the plastic shearing rate $\dot{\gamma}$, can be expressed as the product of $\dot{f}_{tw} \times \gamma_{tw}$, where $\dot{f}_{tw}$ and γ_{tw} are the rate of evolution of twin volume fraction, and twinning shear, respectively. Since the γ_{tw} is constant for a given twin system (0.129 for $\{10\bar{1}2\}$ twinning [2]), the $\dot{\gamma}$ is mainly controlled by the $\dot{f}_{tw}$. An increase in $\dot{\gamma}$ should be accommodated by an increase in $\dot{f}_{tw}$. In the case of samples where twin nucleation occurs easily, the increase in $\dot{f}_{tw}$ is achieved by nucleation of new twins [21]. However, in the current experiment a TB is already present in the sample, and considering lower growth stresses compared to high nucleation stress [40], the increase in $\dot{f}_{tw}$ is only facilitated by an increase in V_{TB}.

Further, it is important to understand the factors that control the V_{TB} as the TB migration has considerable influence on the plastic deformation of Mg alloys. Recent studies show that the precipitate particles can serve as obstacles for TB migration, and the hindering effect depends on the particle density, distribution, shape, and orientation [14–16]. Therefore, V_{TB} is expected to decrease when a moving TB encounters such obstacles. We have carefully re-examined the *in-situ* experiments of Liu et al. [16] and computed the V_{TB} in Mg alloys. For a programed displacement rate of 10 nm/s (twice the displacement rate used in the current study), the V_{TB} in a Mg alloy pillar with dense distribution of LPSO (long period stacking ordered) lamellae is found to be only ~20 nm/s, much less than the V_{TB} observed in the current study. Owing to such low V_{TB}, the plastic strain in Mg alloy pillars could not be accommodated by DT alone, and dislocation slip is necessary [16].

In contrast to the smooth and slow migration of a pre-existing TB in our study, recent experimental investigations indicate a very rapid TB migration following twin nucleation. The formation of twins in micropillars is manifested as pronounced strain bursts which is attributed to rapid twin growth after twin nucleation [5,25,26,29,40]. Sim et al. [29] observed that the magnitude of the strain burst decreases with increasing pillar size, indicating the fact that TB moves quite rapidly in micropillars than the bulk samples. Such difference in V_{TB} can be attributed to the high nucleation stresses observed in micropillars when compared to bulk samples due to strong specimen size effect [41]. In sub-micron pillars, owing to very high twin nucleation stress, the entire gauge part of the sample can even be completely twinned within a single strain burst just after twin nucleation, making it difficult to record the events [5]. However, in our experiments we didn't witness such abrupt twin migration as the specimen already contains a pre-existing TB and no new twin is nucleated. Therefore, TB migration is more controlled and thus enabling us to accurately measure the V_{TB}.

4.4. Tension-compression asymmetry

4.4.1. Tension-compression asymmetry in yield stress and V_{TB}

In all our experiments, it is observed that the yield stress in tension, $\sigma_{y,T}$, is always lower than the yield stress in compression, $\sigma_{y,C}$. In Fig. 7, we have plotted the average tensile and compressive yield stresses (corresponding to twinning and detwinning stresses in this case) against their respective V_{TB} for sample #1. It is interesting to note a higher V_{TB} in tension compared to the compression in spite of lower tensile yield stress compared to the compression. The yield asymmetry, defined as the ratio between the average tensile and compressive yield stresses, $(\sigma_{y,T}/\sigma_{y,C})$ is found to be about 0.8 (Fig. 8). Although yield asymmetry is a commonly observed phenomenon in Mg, it is typically attributed to the activation of different deformation mechanisms and the differences in their CRSS. For example, tension along *c*-axis favors the easy $\{10\bar{1}2\}$ DT while compression along *c*-axis favors the hard non-basal slips [42,43]. However, in current study, yield asymmetry is present despite $\{10\bar{1}2\}$ TB migration is the dominant plastic deformation carrier under both tension and compression.

Another interesting observation, apart from yield asymmetry, is the differences in V_{TB} between the tension and compression. Since V_{TB} is sensitive to strain rate (as discussed in Section 4.3), in order to compare the V_{TB} in different tests, we have defined a normalized V_{TB} which is the ratio of V_{TB} and the actual displacement rate (Table A1). The normalized V_{TB} is plotted against the loading cycle in Fig. 9. Interestingly, the normalized V_{TB} in tension is higher than the compression and it is independent of the loading sequence. This further confirms that $\{10\bar{1}2\}$ TB, indeed, migrates faster under tension than compression. We seek to explain this behavior in the latter subsection with references to the defect environment on

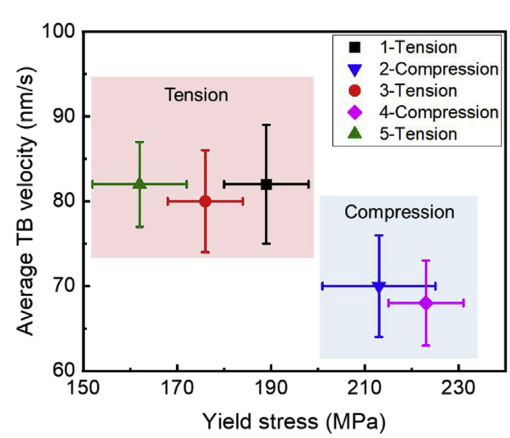

Fig. 7. Variation of average twin boundary velocity, V_{TB} in tension and compression plotted against the respective yield stress values (Sample #1). The differences clearly highlight the differences in V_{TB} during twinning and detwinning.

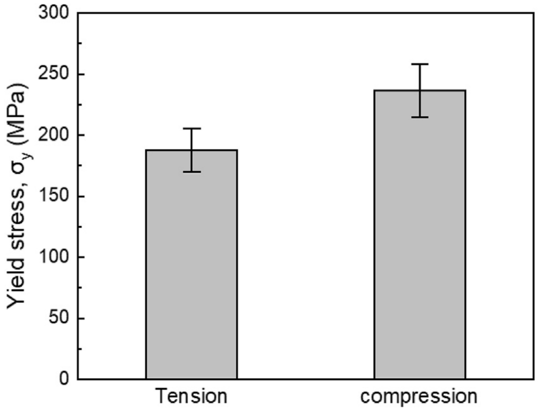

Fig. 8. Summary of average tensile ($\sigma_{y,T}$) and compressive ($\sigma_{y,C}$) yield stresses clearly indicating the tension-compression asymmetry.

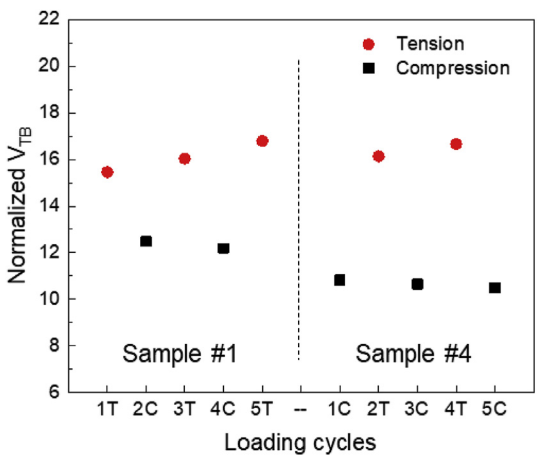

Fig. 9. Normalized V_{TB}, ratio of V_{TB} and displacement rate, clearly indicating that differences in V_{TB} in tension and compression. The first loading of Sample #1 and Sample #4 is tension and compression, respectively.

either side of TB and to the TB structure per se.

4.4.2. Possible mechanism for tension-compression asymmetry

Two possible mechanisms are proposed to be responsible for the observed tension-compression asymmetry (twinning-detwinning asymmetry) in the current experiments. One is due to the differences in defect environment (dislocations, stacking faults (SFs)) on either side of TB, i.e. in matrix and twin, and the other is to BP and PB structures and their number density on TB. Both these mechanisms are discussed below.

4.4.2.1. Defect environment in matrix and twin. Fig. 10a shows the schematic describing the mechanism of CTB migration in a clean crystal containing no defects (e.g. dislocations and SFs) in matrix and twin. The TB migration is mediated by successive movement of twinning dislocations. Under tensile loading, the TB moves towards the matrix (twinning), while during compression it moves towards the twin (detwinning). In both cases, TB migration is accomplished by the movement of twinning dislocations of same kind along the TB but in opposite directions, and no defect obstructs the TB migration, therefore, no asymmetry in the velocity and stress is expected.

Actually, the sample is not a clean crystal. Dislocations exist in the sample and contribute to the plastic deformation (Fig. 6).

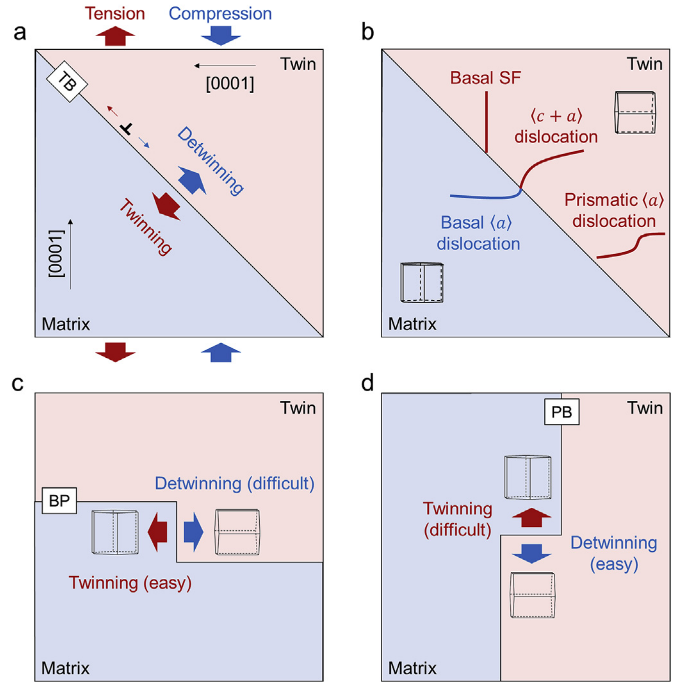

Fig. 10. Schematics illustrating the possible origins of twinning-detwinning asymmetry. (a) Migration of a TB in clean crystal with no defect in matrix and twin. (b) Different defect environment in matrix and twin. (c–d) Migration of BP or PB interface via the movement of a step.

However, the operative slip systems in matrix and twin are expected to be different owing to the differences in their crystallographic orientations. Schmid analysis suggests activation of prismatic $\langle a \rangle$ slip in the twin (Schmid factor, m ~ 0.43) and pyramidal $\langle c+a \rangle$ slip (m ~ 0.4) in both matrix and twin. Although basal $\langle a \rangle$ slip has a negligible Schmid factor, a slight misalignment between the sample and grips can lead to its activation because of the low CRSS. Pyramidal $\langle c+a \rangle$ slip requires very high activation stress [44] thus are not supposed to be largely generated by deformation in the current experiments. Besides plastic deformation, defects can also be introduced associated with TB migration. $\langle a \rangle$ dislocations in matrix can interact with TB and transform into $\langle c+a \rangle$ dislocations in twin via dislocation transmutation [34]. Basal SFs can also be generated in twin after TB sweeping away [34,39]. To summarize, basal $\langle a \rangle$ dislocations can be generated in both matrix and twin, while prismatic $\langle a \rangle$ dislocations, basal SFs and $\langle c+a \rangle$ dislocations can be formed in twin (Fig. 10b). Such differences in defect environment between the matrix and twin could be responsible for the observed tension-compression (twinning-detwinning) asymmetry.

4.4.2.2. TB structure. The $\{10\bar{1}2\}$ TB is usually not a planar CTB but is serrated due to the presence of BP and PB interfaces. The BP and PB interfaces are highly mobile and can potentially influence the TB migration [45–51]. A recent molecular dynamics (MD) simulation study reveals that a BP or PB interface migrates through the motion of a two layers step (corresponds to a HCP unit cell) [51]. Figs. 10c and d represents the schematic of BP and PB interface with such step, respectively. During twinning, BP interface migrates towards matrix causing the transformation of prismatic plane of matrix to basal plane of twin at the step (Fig. 10c) while the motion of PB interface results in the transformation of basal plane of matrix to the prismatic plane of twin at the step (Fig. 10d). During detwinning, the interface migration and transformation of planes are opposite to those in twinning.

Since basal plane more closely-packed than the prismatic plane, it is expected that the basal → prismatic transformation is difficult than the reverse transformation, as observed in recent MD simulation study [46]. Therefore, the motion of BP towards matrix (twinning) is easier than it towards twin (detwinning); on the contrary, the motion of PB towards twin (detwinning) is easier than it towards matrix (twinning), as schematically illustrated in Fig. 10c and d. If BP interfaces are more than the PB interfaces, the twinning is easier than detwinning, vice versa. However, in the current experiments, we cannot accurately obtain the relative proportions of BP and PB interfaces on TB. Therefore, it is difficult to attribute the observed tension-compression (twinning-detwinning) asymmetry completely to the asymmetric nature of BP or PB motion. Moreover, recent MD studies, on HCP Mg and Ti, show the transitory formation of face-centered-cubic (FCC) region at the BP or PB interfaces [52–54]. Whether such FCC region will obstruct TB migration and lead to twining-detwinning asymmetry are worth further investigation.

4.5. Energy absorption by TB migration

Recently experiments of Cui et al. [17,18] reveal that the damping capacity of the Mg alloys can be enhanced by regulating the density and stability of extension twins. They argued that forward and backward motion of TBs absorbs considerable amount of energy and the origins of this are attributed the atomic structure of the TB. Although they emphasize the need to quantify V_{TB} and energy absorption characteristics for improved understanding of the damping properties, they could not measure them due to the limitations associated with the experiment and polycrystalline nature of the specimens. We have computed the energy absorbed due to the TB migration during the cyclic loading by integrating the area under the σ *vs.* ε curve (Fig. 4) and presented in Table 1. The energy measurements reveal that TB migration can absorb considerable amount of energy, in the order of magnitude of 10^7 J/m^3, during both twinning and detwinning. The differences, albeit small, observed in the energies between different tests is mainly due to the differences in the total deformation experienced by the samples. The stress obtained in our test is one order of magnitude than the CRSS for $\{10\bar{1}2\}$ twinning in bulk scale Mg samples [55]. Such high stresses required for TB migration in submicron pillars can account for the obtained high energy dissipation. Our result inspires the design of high-damping devices made by array of submicron Mg fibers containing $\{10\bar{1}2\}$ TBs.

5. Summary

In-situ TEM cyclic loading experiments are carried out on submicron Mg pillars with a focus to understand the dynamics of an individual TB. The experimental results and subsequent analysis, can be summarized as follows.

- The $\{10\bar{1}2\}$ TB in Mg can migrate forward and backward under cyclic loading, corresponding to the twinning and detwinning processes.
- The TB morphology continuously changes during the TB migration.
- The yield stress is found to be higher under compression than tension. The V_{TB} is found to be lower under compression than tension. Such tension-compression (twinning-detwinning) asymmetry is proposed to arise from the different defect environment in matrix and twin and from the TB structure per se.
- The reciprocating TB migration in submicron Mg crystals can absorb considerable energy of about 10^7 J/m^3.

Acknowledgements

This work was supported by the National Key Research and Development Program of China (No. 2017YFB0702001), National Natural Science Foundation of China (Nos. 51601141 and 51621063), 111 Project 2.0 of China (BP2018008), China Postdoctoral Science Foundation (2016M600788), and funding from the Science and Technology Departments of Shaanxi and Xi'an, China (Nos. 2016KTZDGY-04-03, 2016KTZDGY-04-04 and 201805064ZD15CG48). We acknowledge Dr. C.W. Guo, Dr. P. Zhang and D.L. Zhang (Xi'an Jiaotong University) for assistance in sample preparation and TEM experiments. K.E.P would like to thank Prof. Pradeep Mathur, Director, IIT Indore for permitting to visit XJTU during Dec 2017 and Summer 2018. We also appreciate the support from the International Joint Laboratory for Micro/Nano Manufacturing and Measurement Technologies, and the Collaborative Innovation Center of High-End Manufacturing Equipment at Xi'an Jiaotong University, China. Authors declare no competing interests. All data is available in the main text or the supplementary materials.

Appendix

Table A1
4 sets of cyclic loading tests. For Sample #1 to #3, the first loading cycle is tension, while for Sample #4, the first loading cycle is compression. The programmed displacement rate is 5 nm/s. The actual displacement rates applied on samples slightly deviate from the set value due to thermal drift of load device. Data used in Fig. 8 are collected from Samples #1 to #3 (we didn't count the Sample #4 in that plot because the loading device is slightly misaligned so the yield stresses is a little sporadic).

	Loadings	Actual displacement rate (nm/s)	Measured V_{TB} (nm/s)	Normalized V_{TB}
Sample #1 5 cycles	1-Tension	5.34	82.57	15.46
	2-Compression	6.38	79.63	12.48
	3-Tension	5.00	80.17	16.03
	4-Compression	5.91	72.08	12.20
	5-Tension	5.14	86.30	16.79
Sample #2 3 cycles	1-Tension	4.62	69.79	15.11
	2-Compression	6.55	83.90	12.81
	3-Tension	5.18	85.32	16.47
Sample #3 2 cycles	1-Tension	5.32	84.81	15.94
	2-Compression	5.29	70.62	13.35
Sample #4 5 cycles	1-Compression	5.44	58.92	10.83
	2-Tension	2.64	42.60	16.14
	3-Compression	5.22	55.61	10.65
	4-Tension	5.13	85.49	16.66
	5-Compression	5.14	53.84	10.47

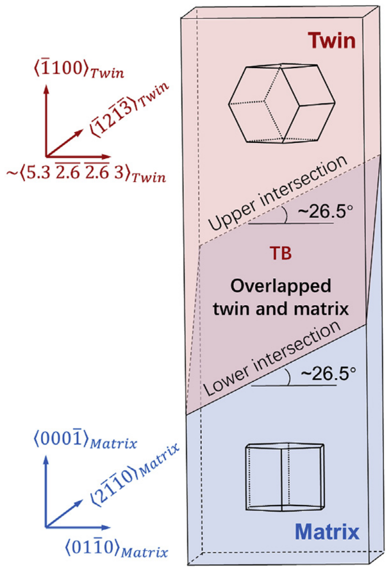

Fig. A1. Schematic showing the geometry of a planar $\{10\bar{1}2\}$ CTB in a square pillar with the same viewing direction used in Figs. 1, 3 and 5.

References

[1] M.H. Yoo, Slip, twinning, and Fracture in hexagonal close-packed metals, Metall. Trans. A 12 (3) (1981) 409–418.
[2] J.W. Christian, S. Mahajan, Deformation twinning, Prog. Mater. Sci. 39 (1995) 1–157.
[3] X.Z. Liao, J. Wang, J.F. Nie, Y.Y. Jiang, P.D. Wu, Deformation twinning in hexagonal materials, MRS Bull. 41 (4) (2016) 314–319.
[4] M.R. Barnett, Twinning and the ductility of magnesium alloys part I: "tension" twins, Mater. Sci. Eng. A 464 (1–2) (2007) 1–7.
[5] B.Y. Liu, J. Wang, B. Li, L. Lu, X.Y. Zhang, Z.W. Shan, J. Li, C.L. Jia, J. Sun, E. Ma, Twinning-like lattice reorientation without a crystallographic twinning plane, Nat. Commun. 5 (2014) 3297.
[6] B.-Y. Liu, L. Wan, J. Wang, E. Ma, Z.-W. Shan, Terrace-like morphology of the boundary created through basal-prismatic transformation in magnesium, Scr. Mater. 100 (0) (2015) 86–89.
[7] M.H. Yoo, C.T. Wei, Growth of deformation twins in zinc crystals, Philos. Mag. 14 (129) (1966) 573–587.
[8] R.E. Cooper, J. Washburn, Stress-induced movement of twin boundaries in zinc, Acta Metall. 15 (4) (1967) 639–647.
[9] Q. Yu, J. Wang, Y. Jiang, R.J. McCabe, C.N. Tomé, Co-zone {10-12} twin interaction in magnesium single crystal, Mater. Res. Lett. 2 (2) (2013) 82–88.
[10] Q. Yu, J. Wang, Y.Y. Jiang, R.J. McCabe, N. Li, C.N. Tome, Twin-twin interactions in magnesium, Acta Mater. 77 (2014) 28–42.
[11] Y. Xin, L. Lv, H. Chen, C. He, H. Yu, Q. Liu, Effect of dislocation-twin boundary interaction on deformation by twin boundary migration, Mater. Sci. Eng. A 662 (2016) 95–99.
[12] J. Zhang, G. Xi, X. Wan, C. Fang, The dislocation-twin interaction and evolution of twin boundary in AZ31 Mg alloy, Acta Mater. 133 (2017) 208–216.
[13] K.D. Molodov, T. Al-Samman, D.A. Molodov, Profuse slip transmission across twin boundaries in magnesium, Acta Mater. 124 (2017) 397–409.
[14] J.D. Robson, The effect of internal stresses due to precipitates on twin growth in magnesium, Acta Mater. 121 (2016) 277–287.
[15] H. Fan, Y. Zhu, J.A. El-Awady, D. Raabe, Precipitation hardening effects on extension twinning in magnesium alloys, Int. J. Plast. 106 (2018) 186–202.
[16] B.-Y. Liu, N. Yang, J. Wang, M. Barnett, Y.-C. Xin, D. Wu, R.-L. Xin, B. Li, R.L. Narayan, J.-F. Nie, J. Li, E. Ma, Z.-W. Shan, Insight from in situ microscopy into which precipitate morphology can enable high strength in magnesium alloys, J. Mater. Sci. Technol. 34 (7) (2018) 1061–1066.
[17] Y.J. Cui, Y.P. Li, S.H. Sun, H.K. Bian, H. Huang, Z.C. Wang, Y. Koizumi, A. Chiba, Enhanced damping capacity of magnesium alloys by tensile twin boundaries, Scr. Mater. 101 (2015) 8–11.
[18] Y.J. Cui, Y.P. Li, Z.C. Wang, Q. Lei, Y. Koizumi, A. Chiba, Regulating twin boundary mobility by annealing in magnesium and its alloys, Int. J. Plast. 99 (2017) 1–18.
[19] Q. Yu, J.X. Zhang, Y.Y. Jiang, Direct observation of twinning-detwinning-retwinning on magnesium single crystal subjected to strain-controlled cyclic tension-compression in 0001 direction, Philos. Mag. Lett. 91 (12) (2011) 757–765.
[20] A. Vinogradov, E. Vasilev, M. Linderov, D. Merson, In situ observations of the kinetics of twinning–detwinning and dislocation slip in magnesium, Mater. Sci. Eng. A 676 (2016) 351–360.
[21] V. Kannan, K. Hazeli, K.T. Ramesh, The mechanics of dynamic twinning in single crystal magnesium, J. Mech. Phys. Solids 120 (2018) 154–178.
[22] M.Y. Zheng, W.C. Zhang, K. Wu, C.K. Yao, The deformation and fracture behavior of SiCw/AZ91 magnesium matrix composite during in-situ TEM straining, J. Mater. Sci. 38 (12) (2003) 2647–2654.
[23] B.M. Morrow, R.J. McCabe, E.K. Cerreta, C.N. Tome, In-situ TEM observation of twinning and detwinning during cyclic loading in Mg, Metall. Mater. Trans. A 45A (1) (2014) 36–40.
[24] K.E. Prasad, K.T. Ramesh, In-situ observations and quantification of twin boundary mobility in polycrystalline magnesium, Mater. Sci. Eng. A 617 (0) (2014) 121–126.
[25] J. Ye, R.K. Mishra, A.K. Sachdev, A.M. Minor, In situ tem compression testing of Mg and Mg-0.2 wt.% Ce single crystals, Scr. Mater. 64 (3) (2011) 292–295.
[26] J. Jeong, M. Alfreider, R. Konetschnik, D. Kiener, S.H. Oh, In-situ TEM observation of {1012} twin-dominated deformation of Mg pillars: twinning mechanism, size effects and rate dependency, Acta Mater. 158 (2018) 407–421.
[27] Q. Yu, L. Qi, K. Chen, R.K. Mishra, J. Li, A.M. Minor, The nanostructured origin of deformation twinning, Nano Lett. 12 (2) (2012) 887–892.
[28] C.A. Volkert, Focused ion beam microscopy and micromaching, MRS Bull. 32 (5) (2007) 389–399.
[29] G.-D. Sim, G. Kim, S. Lavenstein, M.H. Hamza, H. Fan, J.A. El-Awady, Anomalous hardening in magnesium driven by a size-dependent transition in deformation modes, Acta Mater. 144 (2018) 11–20.
[30] X.Y. Zhang, B. Li, X.L. Wu, Y.T. Zhu, Q. Ma, Q. Liu, P.T. Wang, M.F. Horstemeyer, Twin boundaries showing very large deviations from the twinning plane, Scr. Mater. 67 (10) (2012) 862–865.
[31] Y. Liu, N. Li, S. Shao, M. Gong, J. Wang, R.J. McCabe, Y. Jiang, C.N. Tomé, Characterizing the boundary lateral to the shear direction of deformation twins in magnesium, Nat. Commun. 7 (2016) 11577.
[32] Z.-J. Wang, Q.-J. Li, Y.-N. Cui, Z.-L. Liu, E. Ma, J. Li, J. Sun, Z. Zhuang, M. Dao, Z.-W. Shan, S. Suresh, Cyclic deformation leads to defect healing and strengthening of small-volume metal crystals, Proc. Natl. Acad. Sci. 112 (44) (2015) 13502–13507.
[33] H. Fan, S. Aubry, A. Arsenlis, J.A. El-Awady, Discrete dislocation dynamics simulations of twin size-effects in magnesium, MRS Proc. 1741 (2015) mrsf14-1741-aa02-02.
[34] F. Wang, S.R. Agnew, Dislocation transmutation by tension twinning in magnesium alloy AZ31, Int. J. Plast. 81 (2016) 63–86.
[35] F. Wang, K. Hazeli, K.D. Molodov, C.D. Barrett, T. Al-Samman, D.A. Molodov, A. Kontsos, K.T. Ramesh, H. El Kadiri, S.R. Agnew, Characteristic dislocation substructure in1012twins in hexagonal metals, Scr. Mater. 143 (2018) 81–85.
[36] P. Chen, F. Wang, B. Li, Dislocation absorption and transmutation at {1012} twin boundaries in deformation of magnesium, Acta Mater. 164 (2019) 440–453.
[37] F. Wang, C.D. Barrett, R.J. McCabe, H. El Kadiri, L. Capolungo, S.R. Agnew, Dislocation induced twin growth and formation of basal stacking faults in {1012} twins in pure Mg, Acta Mater. 165 (2019) 471–485.
[38] J. Tu, X. Zhang, J. Wang, Q. Sun, Q. Liu, C.N. Tomé, Structural characterization of 101-2 twin boundaries in cobalt, Appl. Phys. Lett. 103 (5) (2013), 051903.
[39] X.Y. Zhang, B. Li, Q. Liu, Non-equilibrium basal stacking faults in hexagonal close-packed metals, Acta Mater. 90 (2015) 140–150.
[40] K.E. Prasad, K. Rajesh, U. Ramamurty, Micropillar and macropillar compression responses of magnesium single crystals oriented for single slip or extension twinning, Acta Mater. 65 (2014) 316–325.
[41] Q. Yu, Z.-W. Shan, J. Li, X. Huang, L. Xiao, J. Sun, E. Ma, Strong crystal size effect on deformation twinning, Nature 463 (7279) (2010) 335–338.
[42] E.W. Kelley, W.F. Hosford, Plane-strain compression of magnesium and magnesium alloy crystals, T. Metall. Soc. AIME 242 (1) (1968) 5–13.
[43] W.B. Hutchinson, M.R. Barnett, Effective values of critical resolved shear stress for slip in polycrystalline magnesium and other hcp metals, Scr. Mater. 63 (7) (2010) 737–740.
[44] B.-Y. Liu, F. Liu, N. Yang, X.-B. Zhai, L. Zhang, Y. Yang, B. Li, J. Li, E. Ma, J.-F. Nie, Z.-W. Shan, Large plasticity in magnesium mediated by pyramidal dislocations, Science 365 (6448) (2019) 73–75.
[45] B. Xu, L. Capolungo, D. Rodney, On the importance of prismatic/basal interfaces in the growth of (1012) twins in hexagonal close packed crystals, Scr. Mater. 68 (11) (2013) 901–904.
[46] J. Wang, L. Liu, C.N. Tomé, S.X. Mao, S.K. Gong, Twinning and de-twinning via glide and climb of twinning dislocations along serrated coherent twin boundaries in hexagonal-close-packed metals, Mater. Res. Lett. 1 (2) (2013) 81–88.
[47] J. Wang, S.K. Yadav, J.P. Hirth, C.N. Tomé, I.J. Beyerlein, Pure-shuffle nucleation of deformation twins in hexagonal-close-packed metals, Mater. Res. Lett. 1 (3) (2013) 126–132.
[48] C.D. Barrett, H. El Kadiri, The roles of grain boundary dislocations and disclinations in the nucleation of {10-12} twinning, Acta Mater. 63 (0) (2014) 1–15.
[49] H. Zong, X. Ding, T. Lookman, J. Li, J. Sun, Uniaxial stress-driven coupled grain boundary motion in hexagonal close-packed metals: a molecular dynamics study, Acta Mater. 82 (0) (2015) 295–303.
[50] J.P. Hirth, J. Wang, C.N. Tomé, Disconnections and other defects associated with twin interfaces, Prog. Mater. Sci. 83 (2016).
[51] Q. Zu, X.-Z. Tang, S. Xu, Y.-F. Guo, Atomistic study of nucleation and migration

of the basal/prismatic interfaces in Mg single crystals, Acta Mater. 130 (2017) 310–318.

[52] J. Ren, Q. Sun, L. Xiao, X. Ding, J. Sun, Phase transformation behavior in titanium single-crystal nanopillars under [0 0 0 1] orientation tension: a molecular dynamics simulation, Comput. Mater. Sci. 92 (2014) 8–12.

[53] P. Chen, F. Wang, B. Li, Transitory phase transformations during {1012} twinning in titanium, Acta Mater. 171 (2019) 65–78.

[54] P. Chen, F. Wang, B. Li, Misfit strain induced phase transformation at a basal/prismatic twin boundary in deformation of magnesium, Comput. Mater. Sci. 164 (2019) 186–194.

[55] N. Stanford, J. Geng, Y.B. Chun, C.H.J. Davies, J.F. Nie, M.R. Barnett, Effect of plate-shaped particle distributions on the deformation behaviour of magnesium alloy AZ91 in tension and compression, Acta Mater. 60 (1) (2012) 218–228.